Ore Geology Reviews 120 (2020) 103393

Contents lists available at ScienceDirect

Ore Geology Reviews

journal homepage: www.elsevier.com/locate/oregeorev

# Geology, Geochemistry and genesis of the Longhua low-temperature hydrothermal Ni-Co arsenide deposit in sedimentary rocks, Guangxi, South China

Wenting Huang[a], Jing Wu[a,b], Huaying Liang[a,*], Xilian Chen[a,c], Jian Zhang[a,d], Long Ren[a]

[a] Key Laboratory of Mineralogy and Metallogeny, Guangzhou Institute of Geochemistry, Chinese Academy of Sciences, Guangzhou 510640, China
[b] College of Resources, Environment and Materials, Guangxi University, Nanning 530004, China
[c] State Key Laboratory of Nuclear Resources and Environment, East China University of Technology, Nanchang 330013, China
[d] Key Laboratory of Environment Change and Resources Use in Beibu Gulf, Ministry of Education, Nanning Normal University, Nanning 530004, China

ARTICLE INFO

*Keywords:*
Mineral exploration
Low-temperature ore
Sedimentary systems
Hydrothermal Ni deposit
South China

ABSTRACT

The Longhua Ni–Co deposit, hosted in Cambrian carbonaceous sandstone and siltstone in South China, consists of disseminated niccolite mineralization and high-grade Ni–Co arsenides–quartz–carbonate vein mineralization. The disseminated mineralization is characterized by niccolite hosted in the center of quartz fragments and in argillaceous concretions in Cambrian banded pisolitic carbonaceous silty mudstone, and by parallel niccolite grains in Cambrian pisolitic pelite. These characteristics indicate that the disseminated niccolite originated through redeposition.

The Ni–Co vein mineralization forms high-grade ores and is composed mainly of Ni–Co-arsenides. The homogenization temperatures of fluid inclusions in the mineralized vein quartz range from 118 to 219 °C, with corresponding salinities of 1.2 to 8.8 wt% NaCl equiv. The ore-forming fluids yield $\delta D_{V\text{-}SMOW}$ (‰) and $\delta^{18}O_{H2O}$ (‰) values of −54 to −66 and −3.0 to −7.7, respectively, indicating that the source was circulating meteoric water. The Longhua Ni–Co vein mineralization gives a niccolite Re–Os isochron age of 462.6 ± 8.5 Ma (MSWD = 1.03).

The geological and geochemical characteristics of the Longhua Ni–Co deposit indicate that it formed as follows. (1) Precambrian quartz–niccolite mineralization was eroded and transported to the Longhua sediment trap, forming low-grade disseminated niccolite mineralization or Ni–Co rich source beds during the Cambrian. (2) High-grade Ni–Co arsenide vein mineralization was formed by further enrichment of Ni–Co from the Ni-rich source beds by circulated meteoric water during the Ordovician (Caledonian orogeny).

The formation of the Longhua low-temperature high-grade Ni–Co vein ore indicates that Ni can be transported in low-temperature fluids that are rich in arsenic and $HCO_3^-$ or $CO_3^{2-}$. The Longhua Ni–Co deposit might represent a new type of sedimentary hosted low-temperature hydrothermal Ni deposit.

## 1. Introduction

Global Ni production is sourced mainly from two deposit types: (1) magmatic Ni deposits, genetically associated with mafic or ultramafic rocks in which the Ni was concentrated by sulfide-rich melts (Arndt et al., 2005; Barnes and Lightfoot, 2005); and (2) lateritic Ni deposits, formed by the weathering of Ni-rich magmatic silicates (e.g. Elias, 2002). Hydrothermal Ni deposits are rarer than magmatic and lateritic Ni deposits, the majority being spatially associated with magmatic Ni deposits or altered ultramafic–mafic rocks (e.g., Gonzalez-Alvarez et al., 2013; Table 1). However, some hydrothermal Ni–Mo deposits have no genetic link with ultramafic–mafic rocks, such as the hydrothermal stratiform black-shale-hosted Ni deposits in Southwest China, which are hosted in a thin stratigraphic horizon of black shale and also contain high concentrations of platinum-group-elements (PGE), Mo, Au, and Zn (Coveney and Nansheng, 1991; Jiang et al., 2006; Lehmann et al., 2007; Mao et al., 2002; Xu et al., 2013) (Fig. 1).

The Longhua Ni–Co deposit in Guangxi Province, Southwest China, is small in scale and comprises quartz–niccolite veins in Cambrian sandstones and siltstones with high concentrations of Ni (> 17%) and Co (1.55%). It has a unique mineral assemblage, where Ni–Co arsenides are the major ore minerals, which differ from that of stratiform black-

* Corresponding author.
*E-mail address:* lianghy@gig.ac.cn (H. Liang).

https://doi.org/10.1016/j.oregeorev.2020.103393
Received 19 February 2019; Received in revised form 22 January 2020; Accepted 5 February 2020
Available online 06 February 2020
0169-1368/ 

**Table 1**
Summerized Characterices of Hydrothermal Ni Deposits.

| Type | Deposit | Location | Host rock | Magmatic Ni sulfides or mafic ultramafic rocks in region | Resources | Ore minerals | References |
|---|---|---|---|---|---|---|---|
| Relate with mafic–ultramafic rocks | Avebury | Tasmania, Australia | Middle Cambrian cumulate peridotite and dunite rocks | Ni-Cu-PGE sulfides at Melba Flats, 24 km to the east of the deposit | 29.3 Mt at 0.9% Ni (0.26 Mt Ni) | Pentlandite with minor pyrrhotite and minor millerite, mackinawith, nickeline, gersdorffite and maucherite | Keays and Jowitt, 2013 |
| | Epoch | Zimbabuwe | Talc-carbonate rocks | Trojan and Shangani NiS deposits | 5.61 Mt at 0.67% Ni, 100 tons of Co, 800 tons of Cu | Pyrite, millerite, bravoite, and minor chalcopyrite and pentlandite | Pirajno and González-Álvarez, 2013 |
| | Doriri Creek | Papuan | Peridotites/pyroxenites within a high MgO noritic gabbro envelope | Papuan ultramafic belt | Average at 1.7 wt% Ni and at 15.1% Ni maximum | Chlorite and serpentine group minerals in addition to Fe oxides, with a minor amount in pentlandite | Gonzalez-Alvarez et al., 2013 |
| | Ishkinino | Urals, Russia | Dunitic and harzburgitic lithologies | Ishkinino and Bayguskarovo complexes | 1.11 Mt at 0.1–0.45 wt%Ni | Chalcopyrite-pyrite-pyrrhotite and Co-Ni-sulfarsenide-sulfide | Melekestseva et al., 2013 |
| | Ivanovka | | Mafic and untramafic volcanic rocks | | 24 Mt at 0.01–0.22 wt% Ni | Pyrite-chalcopyrite-pyrrhotite | |
| | Dergamysh | | Serpentinites and chloritized mafic rocks | | 2 Mt at 0.01–0.35 wt% Ni | Pyrite, marcasite, chalcopyrite and sphalerite | |
| | Bou Azzer | Morocco | Serpentinites | Neoproterozoic ophiolite sequence | 0.15 Mt at 1%Co and 1% Ni | Skutterudite [$CoAs_3$], safflorite [$CoAs_2$], niccolite [NiAs], rammelsbergite [$NiAs_2$], löllingite [$FeAs_2$], cobaltite, gersdorffite, arsenopyrite | Ahmed et al., 2009 |
| | Outokumpu | Finland | Ultramafic massifs | Outokumpu "ophiolite complex" | 28.5 Mt at 0.13% Ni, 0.24% Co | Pyrtie, pyrrhotite, chalcopyrite, sphalerite and minor cobaltian pentlandite, stannite and mackinawite | Peltonen et al., 2008 |
| | Kalumbila (the northeastern end) | Central African | Carbonaceous metapelite | Metagabbros which are anomalous in Ni, Co and Cu | 8Mt at 0.54% Ni, 0.2% Co and 0.14% Cu | Pyrite, chalcopyrite, pyrrhotite, violarite and siegenite. | Steven and Armstrong, 2003 |
| | Tomponson nickel belt | Canada | Serpentinised peridotite and dunite | Ultramafic rocks hosted | 2500 kt Ni,typically has 4–6% Ni in 100% sulfide | Pyrrhotite, pentlandite, and minor chalcopyrite and pyrite | Lightfoot et al., 2017 |
| No link with mafic-ultramafic rocks | Maluhe deposit, Sancha, Wangjiazhai, Ganziping, Chuanyuanping, Houping, Langxi, Daping, Xiaoping and the Cili deposits | SouthChina | Black shales | Not found | Ni + Mo reaching up to 14% | MoSC, pyrite, vaesite, bravoite, millerite, gersdorffite, and jordisite with minor arsenopyrite, chalcopyrite, covellite, sphalerite, tennatite, tiemannite, violarite, and native Au | Xu et al., 2013 |
| | Yukon | Canada | Black shales | Not found | Ni > 0.5% and Mo > 0.2% | Dominantly phosphatic carbonaceous chert and pyrite with lesser amounts of vaesite, melnikovite, spheroids, and jordisite. | Horan et al., 1994 |
| | Talvivaara | North Karelia schist belt, Finland | Middle Cambrian cumulate peridotite and dunite rocks | Altered serpentinite at Lahnaslampi (15 km north) and ophiolitic rocks at Jormua (50 km north). | 1550 Mt at 0.22% Ni and 0.02% Co. | Pyrite, pyrrhotite, sphalerite, chalcopyrite and pentlandite | Loukola-Ruskeeniemi and Lahtinen 2013 |
| | Wittichen | Germany | Triberg granite complex and Buntsandstein redbeds | Not found | 125 tons of Co, 5 tons of Ag | Pitchblende, bismthinite, native A, native Bi, löllingite, rammelsbergite, nickeline, pararammelsbergite, rammelsbergite, gersdorffite, skutterudite, chalcopyrite, wittichenite and aikinite. | Staude et al., 2012 |
| | Enterprise | Zambia | Neoproterozoic metasedimentary rocks | Minor Mafic meta-igneous rocks | 40Mt at 1.07% Ni | Bravoite, vaesite, millerite, pyrite, chalcopyrite, molybdenit, pyrrhotite and carrollite. | Capistrant et al., 2015 |

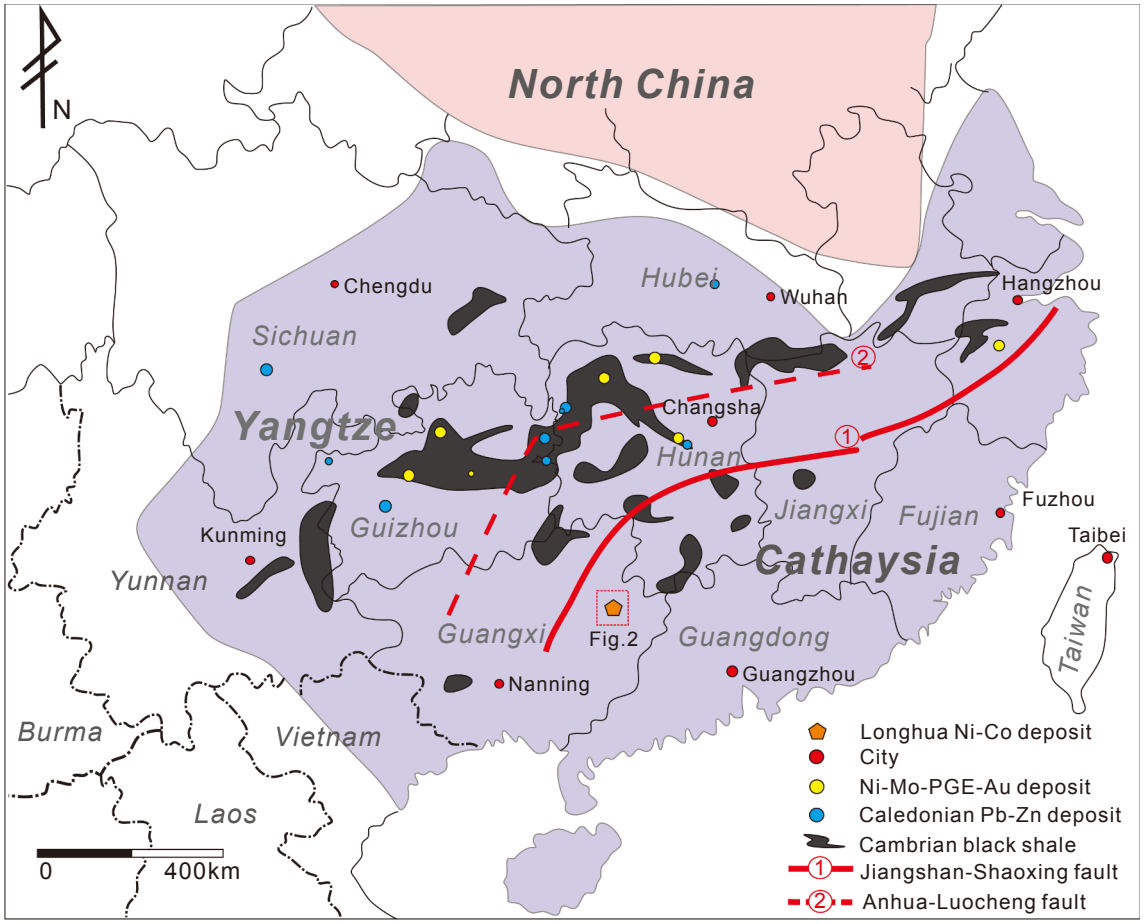


**Fig. 1.** Simplified geological map of the South China Block and the locations of polymetallic Ni–Mo–PGE–Au deposits hosted in black shale (modified after Mao et al., 2002; Wang et al., 2013).

shale-hosted Ni deposits in Southwest China that consist mainly of $[Mo,Fe,Ni][S,As]_2C_7$, vaesite, bravoite, and jordisite (Jiang et al., 2006). In this study, we describe the geological features of the Longhua Ni–Co deposit, and we present Re–Os isochron age data for the niccolite together with temperature and H–O isotopic composition data for the ore-forming fluids. The aim of this work is to establish the nature of the genetic processes involved in the formation of the Longhua Ni–Co deposit and discuss whether it is a new type of low-temperature hydrothermal Ni deposit. Our study provides an example of a low temperature (< 200 °C) hydrothermal Ni-Co deposit that formed over several mineralizing events, and shows how this differs from hydrothermal Ni deposits that form at temperatures of 250–600 °C. Our work also emphasizes the effects of $As^-$ and $CO_2/HCO_3^-$ on Ni mobility and solubility in low temperature environments.

## 2. Geological background

The South China Block (SCB) consists of the Yangtze Block in the northwest and the Cathaysia Block in the southeast, separated by the NE-striking Jiangshan–Shaoxing Fault (Fig. 1; Charvet et al., 1994; Huang et al., 1980; Wang et al., 2010), formed during the Jinningian subduction–collision event at 1000–860 Ma (Charvet et al., 1996; Li and McCulloch, 1996). The relationship between the Yangtze and Cathaysia blocks following the Jinningian subduction–collision event is less clear. Some researchers suggest that the SCB remained intact (Li et al., 2010a; Wang et al., 2006; Xu et al., 2000), whereas others have argued that the SCB rifted apart along the line of Hunan–Jiangxi–western Guangdong–eastern Guangxi provinces during the breakup of Rodinia (after ~800 Ma), forming the early Paleozoic Huanan Ocean (Hsü et al., 1990; Wang and Li, 2003) or an intercontinental basin (Wang et al., 2006), and reassembled during the middle Paleozoic (Hsü et al., 1990; Liu and Xu, 1994). The SCB has experienced at least four major tectonic events since ~1000 Ma; i.e., the Jinningian (~970 Ma; Charvet et al., 1996), Ordovician–Devonian Caledonian, late Permian–Triassic Indosinian (Wang et al., 2006), and Jurassic–Cretaceous Yanshanian tectonic events (eg. Li and Li, 2007). The Jinningian tectonic event resulted in Proterozoic subduction–collision between the Yangtze and Cathaysian blocks, resulting in the formation of the Jiangshan–Shaoxing Fault (Fig. 1; Charvet et al., 1996). The Caledonian tectonic event involved intracontinental collision that induced Ordovician–Devonian magmatism, crustal thickening, and ductile deformation (Charvet et al., 2010; Chen et al., 2018; Li et al., 2010a). The Indosinian tectonic event probably resulted from intracontinental orogenesis triggered by far-field stress resulting from collisions between the Indochina and South China blocks, and between the North China and South China blocks (Chen, 1999; Gao et al., 2017), which led to crustal thickening and Triassic magmatism (Huang et al., 2017; Wang et al., 2013; Wu et al., 2012). The Yanshanian event was initially triggered by subduction of the Paleo-Pacific plate, followed by breakup and rollback of the subducted Pacific plate (198–90 Ma), which induced widespread magmatism and NNE-trending faults in the Cathaysia Block (Huang et al., 2018; Li, 2000; Li and Li 2007; Li et al., 2018; Mao et al., 2013).

The crystalline basement rocks of the Yangtze block yield zircon U–Pb ages of 3.2–1.8 Ga (Gao et al., 1999; Qiu et al., 2000; Zheng et al., 2006). The Cathaysian basement is largely Paleoproterozoic in age (2.0–1.8 Ga) and is composed of greenschist- to lower amphibolite-facies gneisses, migmatites, and plagioclase amphibolites. In the SCB,

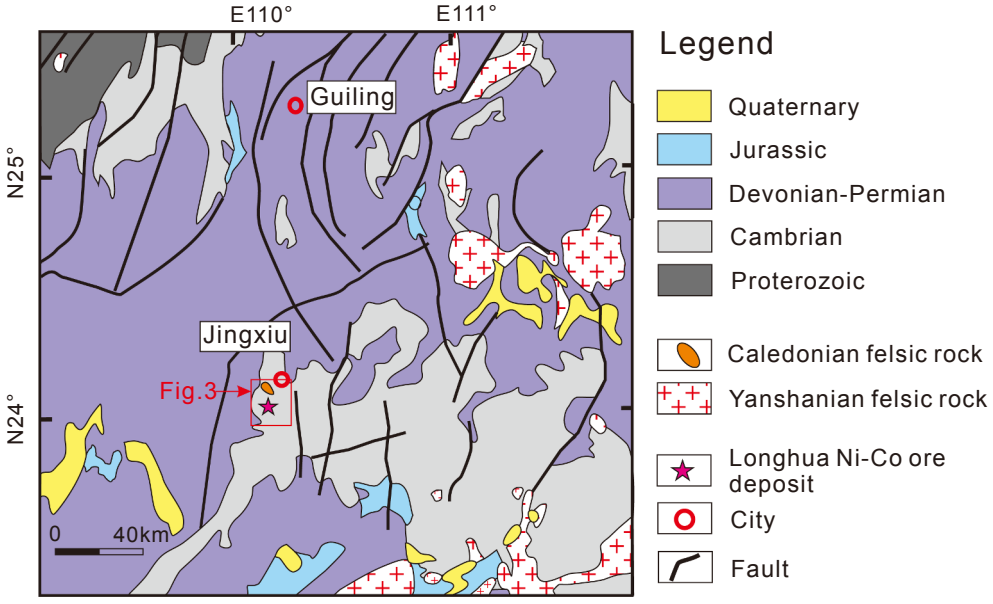


**Fig. 2.** Schematic regional geology map of the Longhua Ni–Co deposit.

Neoproterozoic–Ordovician sediments unconformably or pseudo-conformably overlie basement rocks and are themselves unconformably overlain by Middle–Upper Devonian strata (Xu et al., 2013). The early Cambrian black shale (Niutitang Formation and stratigraphic equivalents; Zhu et al., 2003) that unconformably overlies the Neoproterozoic Dengying and stratigraphically equivalent formations are found in a belt extending across Yunnan, Guizhou, Guangxi, Hunan, Jiangxi, Anhui, and Zhejiang provinces (Fig. 1; Chen et al., 1982; Mao et al., 2002; Zhu et al., 2003). The black shale sequences are rich in organic matter (C, S and P), which possibly formed in anoxic, sediment-starved euxinic basins along the passive margin of the Yangtze Block (McKerrow et al., 1992; Steiner et al., 2001). A series of polymetallic Ni–Mo–PGE–Au sulfide ores or ore occurrences (Re–Os ages of 560–532 Ma) are hosted in the lower Cambrian black shale along a 1,600 km-long, NE-SW trending belt in the eastern Yangtze Block (Fig. 1; Xu et al., 2013). The ore minerals consist mainly of MoSC phase ($[Mo,Fe,Ni][S,As]_2C_7$), vaesite, bravoite, and jordisite, with minor sulfides (Jiang et al., 2006). Previous studies indicated that the ore-forming fluids were derived from submarine hydrothermal fluids (Steiner et al., 2001; Jiang et al., 2006) or seawater (Mao et al., 2002; Lehmann et al., 2007).

Numerous Pb-Zn deposits are hosted in Neoproterozoic to lower Cambrian strata in Sichuan, Yunnan, Guizhou, Hunan, and Hubei provinces. These deposits were formed during the Caledonian (Fig. 1), and yield Rb-Sr isochron ages ranging from ca. 410 Ma to 490 Ma (Duan et al., 2014; Cao et al., 2015; 2018; Yang et al., 2015; Yu et al., 2017; Du et al., 2018; Tan et al., 2018; Wang et al., 2018; Xiong et al., 2018). The mineralization was considered by Xiong et al. (2018) to be Mississippi Valley type (MVT), and related to the collision between the North China and South China blocks.

The Longhua Ni–Co deposit is located in the interior of the Cathaysia Block, ~300 km northeast of the well-known stratiform black-shale-hosted Ni–Mo–PGE–Au ore deposits of the SCB (Fig. 1; Coveney and Nansheng, 1991; Jiang et al., 2006; Lehmann et al., 2007; Mao et al., 2002) and the Caledonian MVT Pb-Zn deposits (Fig. 1).

## 3. Regional geological context

The exposed strata in the Longhua deposit and adjacent area consist mainly of middle–late Proterozoic greenschist-facies metamorphic rocks, Cambrian low-grade metamorphic rocks, and Devonian sandstone and siltstone (Fig. 2). The upper units of the middle–late Proterozoic occur in the northwestern part of the region, > 100 km away from the Longhua deposit (Fig. 2). The units consist of black shale, siliceous rocks, and siliceous shale interlayered with dolomite. These rocks contain locally lenticular phosphate ore and coal, and are enriched in Ni, Mo, and V (GXBGMR, 1985). The Cambrian rocks are composed of coarse sandstone, fine sandstone interlayered with siltstone, pisolitic pelite, and banded pisolitic carbonaceous pelite, all of which have undergone low-grade metamorphism (GXBGMR, 1985). Three layers of carbonaceous pelite occur in the middle Cambrian basement, and Jurassic–Cretaceous siltstones and sandy conglomerates occur sporadically in the north and south of the ore field (Fig. 2).

There is no evidence of active magmatism, and no ultramafic or mafic rocks are found in the region (Figs. 2 and 3A). Most of the felsic intrusions are Yanshanian in age (GXBGMR, 1985) and are exposed within 100 km northeast and southeast of the Ni deposit, with the Dishui granite being the only felsic igneous intrusion within the ore field (Figs. 2 and 3A). Major faults in the region are NE–SW-trending, with minor N–S- and E–W-trending faults (Fig. 2).

The Longhua Ni–Co deposit was discovered in 2010 (Li et al., 2010b). Eight veins comprise the ore field, one of which has a proven reserve of 3226 t of Ni at an average grade of 17.55% and 285 t of Co at an average grade of 1.55% (December 2016 data, unmined resource). The known mineralization depth of the ore vein is above 80 m depth in one of the veins, and the mineralization in the remaining seven veins is under-explored. Anomalous enrichment of nickel occur over a strike length of > 1.8 km long (Fig. 3A), so the potential for additional discoveries of mineralization at Longhua remains incompletely understood.

The Longhua Ni–Co deposit contains disseminated Ni mineralization (Fig. 3B, Fig. 4) and Ni–Co vein mineralization (Fig. 3B, Figs. 5 and 6).

The main ore mineral of the disseminated Ni mineralization is niccolite. This mineralization occurs predominantly in the Cambrian banded pisolitic carbonaceous silty mudstone and the banded pisolitic carbonaceous pelite. In the former, niccolite grains occur mainly in argillaceous concretions (Fig. 4A) or are hosted by quartz fragments (Fig. 4B). In the pisolitic pelite, the niccolite are occurred as isolated grains, which are aligned with each other (Fig. 4C). The scale of the disseminated mineralization is largely unknown, as disseminated niccolite is only observed in a small exploration tunnel.

The Ni–Co vein mineralization occurs predominantly as Ni–Co arsenides–quartz–calcite veins (Figs. 5 and 6) that dip to the NNE in the

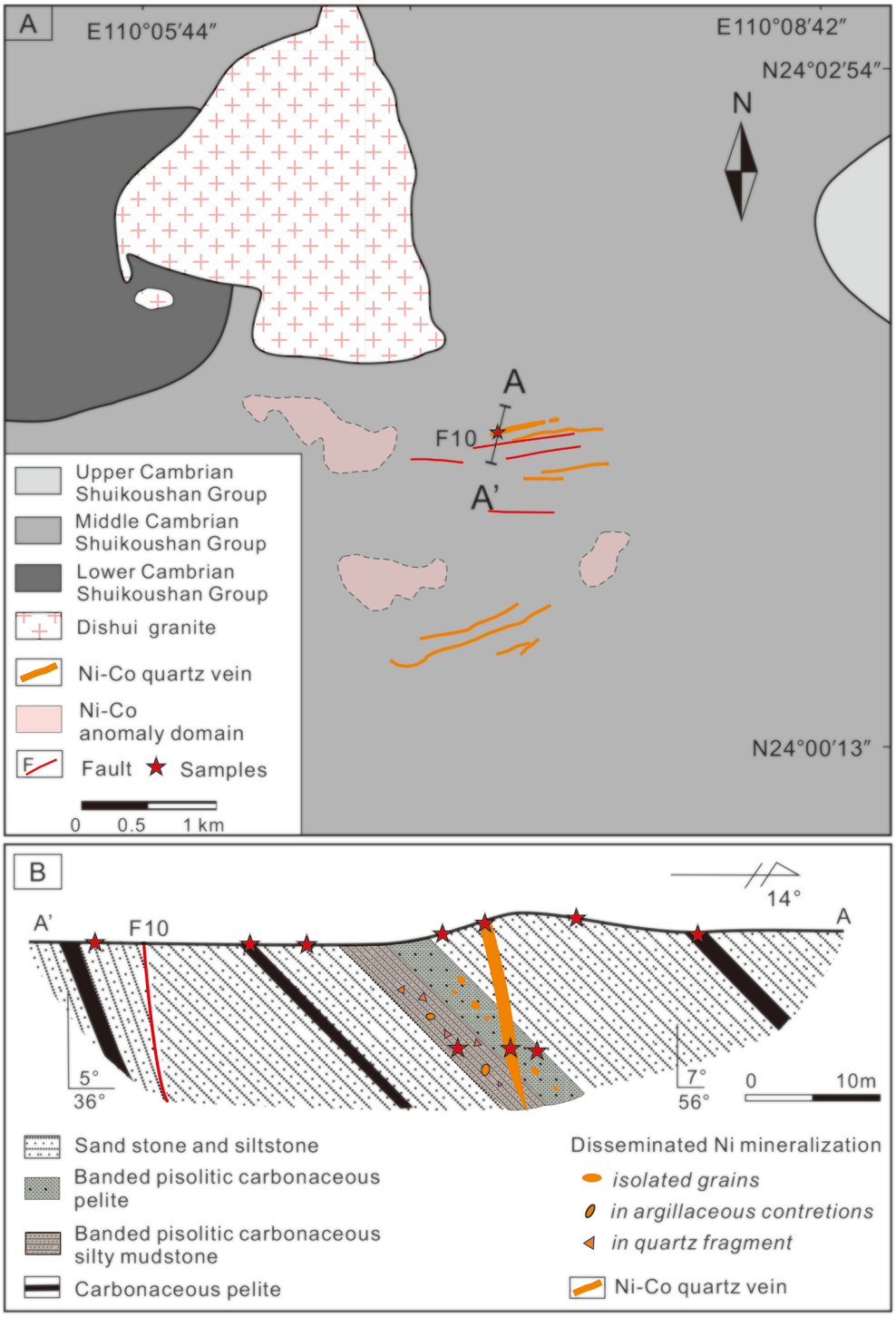


**Fig. 3.** (A) Simplified geological map of the Longhua Ni–Co deposit in Jinxiu County, Guangxi, China. A–A' indicates the location of the cross-section shown in Fig. 3B. (B) Schematic cross-section of the line A–A'.

Cambrian sandstones and siltstones (Fig. 3B). Eight ore veins have been found in the Longhua ore field (Fig. 3A). The largest vein dips at 70°, is ~128 m long, and 1 m thick. The predominant ore mineral is niccolite (NiAs), with minor amounts of gersdorffite [(Ni, Co)AsS], maucherite ($Ni_{11}As_8$), cobaltite [(Co, Ni)AsS)], pentlandite [(Ni, Fe)S], skutterudite [(Co, Ni)$As_2$], chloanthite [(Ni, Co)$As_2$], parkerite ($Ni_3Bi_2S_2$) (these minerals are identified by electron probe analysis), chalcopyrite, pyrite, and arsenopyrite (Fig. 6). The gangue minerals are quartz, chalcedony, calcite, and sericite. Silica, carbonate, and sericite alteration is associated with the Ni–Co mineralization.

The Longhua vein mineralization can be further subdivided into two periods based on evidence that later vein mineralization cross-cuts early vein mineralization (Fig. 6E, F). The later mineralization is characterized by small veins or veinlets and is only found locally in the ore veins, suggesting that the Longhua Ni–Co vein ore is composed primarily of early period mineralization, which yields a mineral assemblage of niccolite with minor gersdorffite, maucherite, pentlandite, chalcopyrite, and pyrite (Fig. 6C, D). The late period mineralization contains more gersdorffite, cobaltite, skutterudite, and parkerite (Fig. 6E, F), suggesting that the Co content increases over time.

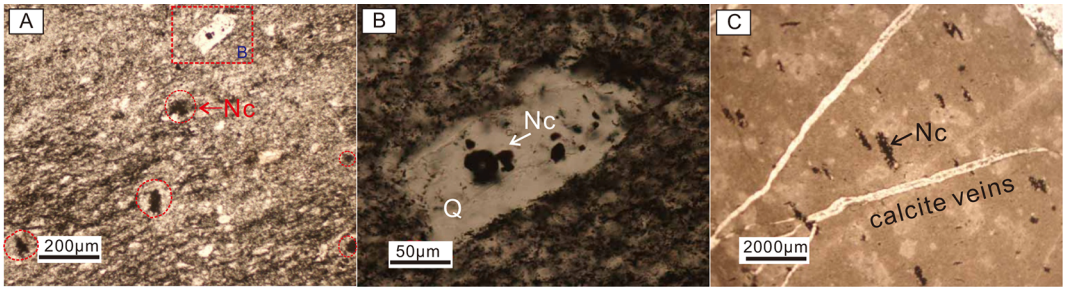


**Fig. 4.** Representative photomicrographs showing disseminated Ni-mineralization in the Longhua Ni–Co deposit: (A) niccolite hosted in quartz fragments and in argillaceous concretions in silty mudstone; (B) high-magnification view of a niccolite-bearing quartz fragment; and (C) aligned niccolite grains in pisolitic pelite. Abbreviations: Nc = niccolite; Q = quartz.

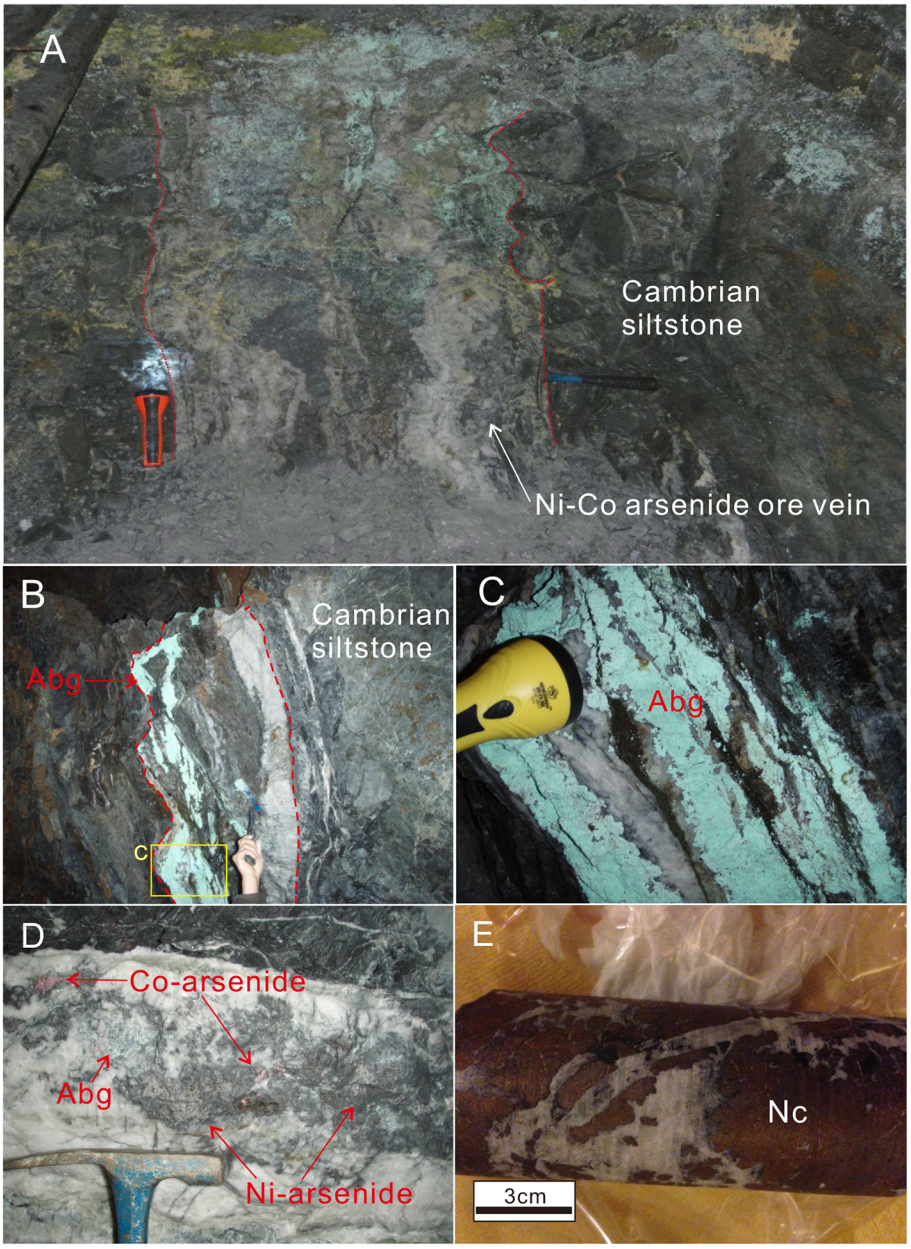


**Fig. 5.** Representative photographs showing Ni–Co vein mineralization: (A) Ni–Co arsenide–quartz–calcite vein cross-cutting Cambrian siltstone; (B) surface of Ni arsenide altered to annabergite; (C) high-magnification view of annabergite; (D) Ni-arsenide (annabergite) and minor Co-arsenide ore associated with quartz–calcite gangue; and (E) representative hand specimen of high-grade Ni–Co ore from drillcore. Abbreviations: Abg = annabergite; Nc = niccolite.

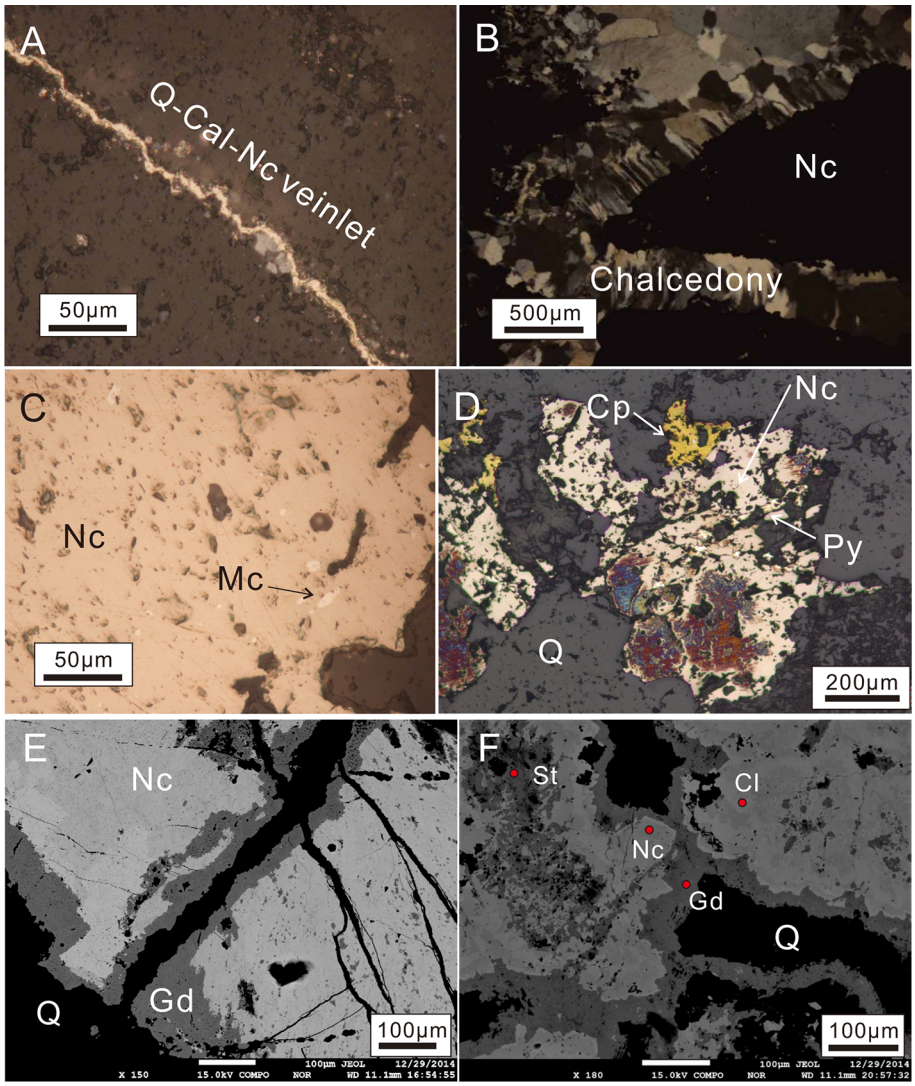


**Fig. 6.** Representative photomicrographs of samples from the study area: (A) reflected-light photomicrograph of a niccolite–calcite veinlet; (B) association of niccolite and chalcedony, suggesting low-temperature mineralization; (C) early stage Ni-vein mineralization of niccolite and minor maucherite; (D) early stage Ni-vein mineralization of niccolite with minor chalcopyrite and pyrite; (E) Co-bearing gersdorffite–quartz vein cutting niccolite; and (F) late-stage Ni–Co vein mineralization comprising gersdorffite, chloanthite, niccolite, and skutterudite. Abbreviations: Cal = calcite; Cl = chloanthite; Cp = chalcopyrite; Gd = gersdorffite; Mc = maucherite; Nc = niccolite; Py = pyrite; Q = quartz; St = skutterudite.

## 4. Sampling and analytical methods

### 4.1. Sampling

To constrain the features of the ore-forming fluids and timing of mineralization, we collected 32 samples from the largest Ni-Co arsenide-quartz-calcite vein in the Luonghua ore field (Fig. 3) and 39 samples from ore-hosting rocks in a small exploration tunnel and from drill cores. Twelve quartz samples from the vein were selected for fluid inclusion analysis, and six quartz samples were chosen for H–O isotope analysis. Six niccolite separates from the vein were used for Re–Os dating.

### 4.2. Fluid inclusions

Fluid inclusion microthermometry was carried out at the Guangzhou Institute of Geochemistry, Chinese Academy of Sciences, Guangzhou, China, using a Linkam MDSG600 heating–freezing stage with Zeiss microscope optics. Measurements were taken at heating and cooling rates of < 10 °C/min and < 1 °C/min, respectively. The estimated accuracy of the microthermometry measurements is ± 2 °C for homogenization temperatures (Th) and ± 0.1 °C for last ice melting temperatures. The salinity of fluid inclusions was calculated based on the final ice melting temperatures according to the equation for the NaCl–$H_2O$ binary system provided by Bodnar (1993).

### 4.3. H–O isotopes

Samples picked from mineralized veins were first crushed to 40–60 mesh. Quartz was separated by heavy liquid separation and then handpicked under a binocular microscope until purity exceeded 99%. For O isotope analyses, the purified quartz samples were powdered to ~200 mesh. Samples of 5–10 g of powdered quartz were analyzed. Oxygen was extracted using $BrF_5$ based on the method described by Clayton and Mayeda (1963). The extracted $O_2$ was reacted with graphite to produce $CO_2$. For H isotope analyses, 3–6 g quartz was placed in an induction furnace to decrepitate the fluid inclusions, and the $H_2O$ was reduced with Zn metal in a sealed tube at 400 °C (Coleman et al., 1982). The H and O isotopic compositions were measured at the Analytical Laboratory, Beijing Research Institute of Uranium Geology, Beijing, China, using a MAT-253EM stable isotope mass spectrometer. Analytical precisions of H and O isotopic measurements are 1 per mil and 0.2 per mil, respectively. The $\delta^{18}O$ and δD values are given relative to V-SMOW (Baertschi, 1976).

### 4.4. Niccolite Re–Os isotopic composition

The niccolite was handpicked under a binocular microscope to purity of > 99%. Re–Os isotope analyses were carried out in the State Key Lab of Ore Deposit Geochemistry, Institute of Geochemistry, Chinese Academy of Sciences, Guiyang, China, following the procedure of Qi et al. (2010). Re–Os isotopes of niccolite were measured using the

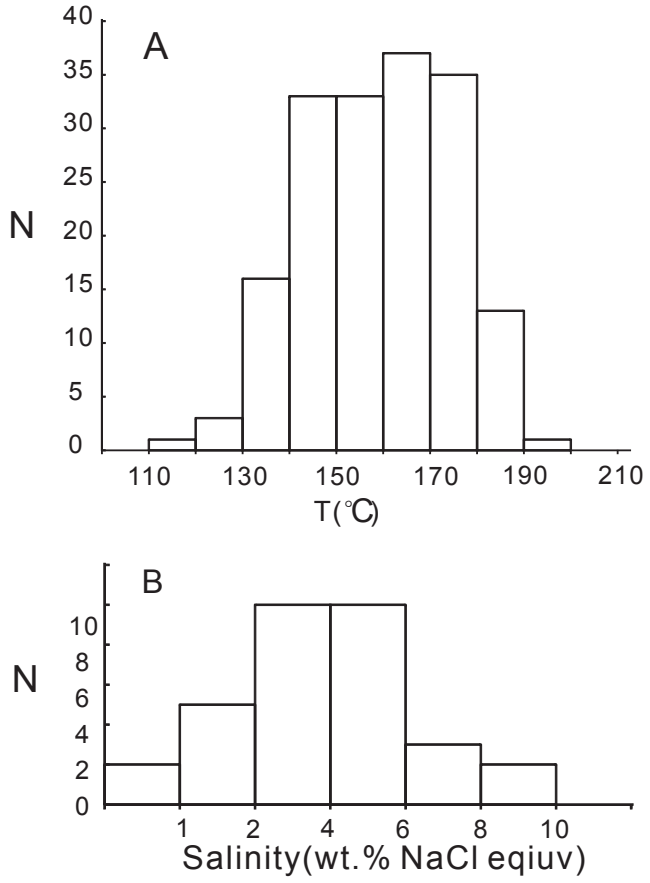


**Fig. 7.** Histograms of (A) homogenization temperatures and (B) salinities of fluid inclusions from the Longhua vein mineralization.

**Table 2**
H-O Isotopic Compositions of Fluids in Longhua Ni Deposit.

| Sample No. | Mineral | $\delta^{18}O_{V\text{-}SMOW}$ (‰) | T(°C) | $\delta^{18}O_{H2O}$(‰) | $\delta D_{V\text{-}SMOW}$ (‰) |
|---|---|---|---|---|---|
| LH14-13–3 | quartz | 13.9 | 160 | −3.0 | −61 |
| LH14-14 | quartz | 12.7 | 156 | −4.5 | −54 |
| LH11-1 | quartz | 12.5 | 160 | −4.4 | −54 |
| 16JX-05–2 | quartz | 13.6 | 131 | −6.2 | −61 |
| 16JX-05–1 | quartz | 13.1 | 131 | −6.7 | −65 |
| 16JX-03 | quartz | 12.4 | 128 | −7.7 | −66 |
| 16JXzk7201-01 | quartz | 11.7 | 143 | −6.8 | −62 |

ID–TIMS method following the procedures of Selby and Creaser (2001). The full procedural blanks for Re and Os were 2 pg and 0.5 pg, respectively, and all Re and Os data were blank corrected. Rhenium ($^{187}$Re) and $^{187}$Os abundances were determined to calculate Re–Os model ages using a $^{187}$Re decay constant of $1.666 \times 10^{-11}$ $a^{-1}$ (Smoliar et al., 1996). The Re–Os isochron ages were calculated using the program ISOPLOT (Ludwig, 2003).

## 5. Results

### 5.1. Fluid inclusions

Quartz from the Ni–Co veins contains primary and secondary fluid inclusions. Primary fluid inclusions are aligned along growth zones within individual quartz crystals, or occur as scattered and isolated inclusions in the quartz. The secondary fluid inclusions occur in trails that cut mineral grain boundaries and have features similar to those described by Roedder (1984).

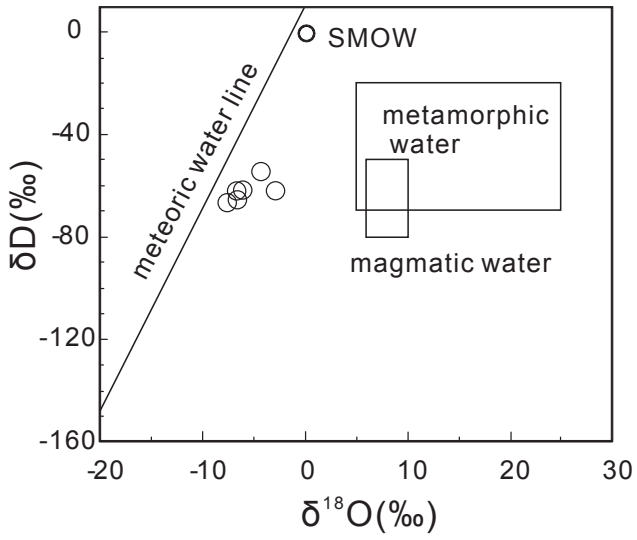


**Fig. 8.** H–O isotopes of fluid inclusions in quartz from the Longhua Ni–Co vein mineralization.

Primary fluid inclusions are ellipsoids or negative crystals with diameters of 5 to 15 μm. They are mainly two-phase inclusions, with vapor/liquid ratios of < 10% at room temperature. Measured homogenization temperatures of 172 primary fluid inclusions vary from 118 to 219 °C, with a peak at 150–182 °C (n = 105, Fig. 7A). The final ice melting temperatures range from −0.7 to −5.7 °C, with corresponding salinities of 1.2–8.8 wt% NaCl equiv. (Fig. 7B).

### 5.2. H–O isotopes

Hydrogen and O isotopic compositions of seven quartz samples from Ni–Co arsenides–quartz–calcite veins were analyzed and are listed in Table 2. The quartz samples have $\delta D_{V\text{-}SMOW}$ and $\delta^{18}O_{V\text{-}SMOW}$ values of −54‰ to −66‰ and 11.7‰ to 13.9‰, respectively, with calculated $\delta^{18}O_{H2O}$ values of −3.0‰ to −7.7‰. In the $\delta D_{V\text{-}SMOW}$ (‰) vs. $\delta^{18}O_{H2O}$ (‰) diagram, the samples plot near the meteoric water line (Fig. 8).

### 5.3. Niccolite Re–Os isotopic composition

Niccolite Re–Os isotopic compositions of the Longhua Ni–Co veins are listed in Table 3. Seven niccolite samples have Re and common Os concentrations of 4.34–52.92 ppb and 4.1–8.7 ppt, respectively. The niccolite samples have relatively high $^{187}$Re/$^{188}$Os (4926–33,713) and $^{187}$Os/$^{188}$Os (38.9–253.1) values, with $^{187}$Os accounting for 84%–97% of the total Os. As discussed by Stein et al. (2000), the best way to represent results from highly radiogenic samples is to plot radiogenic $^{187}$Os vs. $^{187}$Re. Seven niccolite samples define a Re–Os isochron age of 462.6 ± 8.5 Ma (MSWD = 1.03; Fig. 9). The initial $^{187}$Os content of 0.00025 ± 0.00066 is indistinguishable from zero, indicating that the plotted $^{187}$Os concentrations are derived solely from $^{187}$Re decay since niccolite formation. The isochron age and model ages (482–458 Ma; average 466 Ma) agree within error.

## 6. Discussion

### 6.1. Genesis of disseminated mineralization

In the disseminated mineralization of the Longhua Ni–Co deposit, niccolite occurs mainly in the following three forms: (1) niccolite hosted in quartz fragments; (2) parallel niccolite grains in the Cambrian banded pisolitic carbonaceous pelite; and (3) niccolite associated with argillaceous concretions in the Cambrian banded pisolitic carbonaceous silty mudstone without observed alteration.

**Table**
3 Re-Os Data for Niccolite from Longhua Ni-Co Deposit.

| Sample No. | Weight(g) | Re (ppb) | ± 1σ | Common Os(ppt) | ± 1σ | $^{187}$Re | ± 1σ | $^{187}$Os(ppt) | ± 1σ | $^{187}$Re/$^{188}$Os | ± 1σ | $^{187}$Os/$^{188}$Os | ± 1σ | %$^{187}$Osr | t(Ma) | ± 1σ |
|---|---|---|---|---|---|---|---|---|---|---|---|---|---|---|---|---|
| P23-1 | 1.0562 | 11.68 | 0.23 | 5.74 | 0.17 | 7.31 | 0.15 | 57.17 | 0.61 | 9589 | 338 | 74.9 | 1.8 | 91% | 469 | 5 |
| P23-3 | 1.1023 | 10.33 | 0.17 | 6.34 | 0.39 | 6.46 | 0.11 | 51.93 | 0.38 | 7668 | 488 | 61.8 | 3.5 | 89% | 482 | 4 |
| P23-4 | 1.0841 | 35.27 | 0.49 | 5.32 | 0.27 | 22.08 | 0.31 | 168.86 | 2.27 | 31,200 | 1615 | 230.7 | 11.4 | 97% | 459 | 6 |
| P23-2 | 1.1106 | 52.92 | 0.57 | 7.39 | 0.29 | 33.13 | 0.35 | 252.96 | 3.04 | 33,713 | 1373 | 253.1 | 8.7 | 97% | 458 | 5 |
| 14–22-1 | 1.0235 | 17.66 | 0.28 | 8.03 | 0.28 | 11.05 | 0.17 | 84.95 | 1.43 | 10,354 | 401 | 79.9 | 2.3 | 91% | 461 | 8 |
| 14–22-2 | 1.0645 | 31.07 | 0.38 | 8.66 | 0.30 | 19.45 | 0.24 | 151.62 | 0.96 | 16,882 | 623 | 130.6 | 3.8 | 95% | 468 | 3 |
| 14–22-5 | 1.2142 | 4.34 | 0.04 | 4.14 | 0.14 | 2.72 | 0.02 | 21.17 | 0.14 | 4926 | 171 | 38.9 | 1.4 | 84% | 468 | 3 |

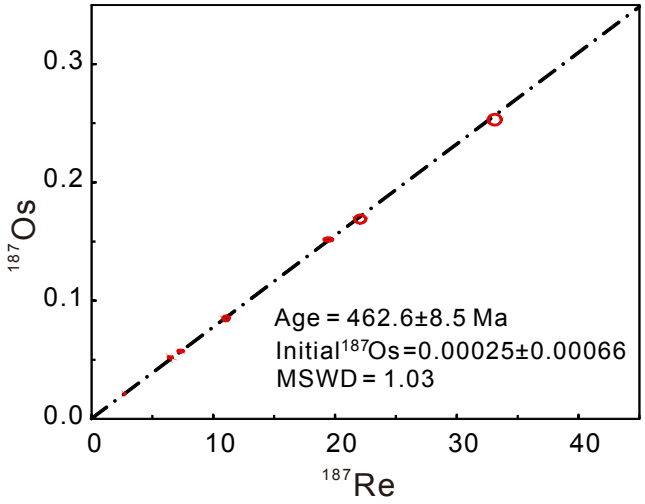


**Fig. 9.** Re–Os isochron age of niccolite from the Longhua Ni–Co deposit.

The niccolite grains in the quartz fragments might have crystallized from ore-forming fluids that entered the quartz fragments during vein mineralization. However, this would require channels for the ore forming fluids to enter the center of the quartz fragments, and given that there were no connecting channels in the quartz fragments, and no niccolite mineralization was found surrounding the quartz fragments, we can reject this process as a means for niccolite formation in the Longhua Ni–Co deposit. Alternatively, niccolite-bearing quartz fragments may have been derived from pre-existing quartz–niccolite ore veins that were eroded and transported from elsewhere, and co-deposited with the Cambrian sediments, forming disseminated niccolite in the Cambrian banded pisolitic carbonaceous silty mudstone and pelite. This redeposition process is supported by the presence of disseminated niccolite grains that are aligned parallel to each other, and niccolite associated with argillaceous concretions in the Cambrian pelite and silty mudstone (Fig. 4). Overall, the distribution of the disseminated niccolite suggests that the disseminated niccolite mineralization was reworked and re-deposited during the Cambrian.

### 6.2. Characteristics and sources of the ore-forming fluids

The fluid inclusions in quartz from the Ni–Co arsenides–quartz–calcite veins yield homogenization temperatures of 118–198 °C, with a peak at 150–182 °C. Their salinities range from 1.2 to 8.8 wt% NaCl equiv. These results suggest that the Ni vein mineralization in the Longhua deposit precipitated from low-temperature, low-salinity fluids. The low-temperature mineralization is consistent with the mineral assemblage of niccolite + chalcedony + calcite (Fig. 7B).

The H and O isotopic compositions of the ore forming fluids in the Ni–Co vein mineralization plot adjacent to the line of meteoric water in the $\delta D_{V\text{-}SMOW}$(‰) vs. $\delta^{18}O_{H2O}$(‰) diagram, suggesting that the ore-forming fluids were sourced mainly from circulating meteoric water that had interacted with the source rocks. Therefore, the formation of the Longhua Ni–Co hydrothermal deposit was related to low-temperature, low-salinity, circulating meteoric water.

### 6.3. Formation of high–grade Ni–Co ore veins

#### 6.3.1. Age of high-grade Ni–Co ore veins

The niccolite from the Ni–Co arsenides–quartz–calcite veins yields a Re–Os isochron age of 462.6 ± 8.5 Ma (MSWD = 1.03; Fig. 9), suggesting the Ni–Co vein mineralization formed during the Ordovician, after the disseminated Ni mineralization, which formed during the Cambrian. The Longhua Ni–Co deposit can therefore be divided into early stage disseminated mineralization and late-stage vein mineralization. The Ni sources of hydrothermal Ni deposits worldwide is mainly mafic igneous rocks or Ni-sulfide deposits (Table 1). However, no mafic rocks are associated with the Longhua Ni–Co deposit or present in the surrounding areas. We propose that the re-deposition of niccolite disseminated in the Cambrian strata could have provided a favorable Ni (–Co) source for the high-grade Ni–Co vein ore.

Heat is also a fundamental requirement for a hydrothermal system. Ore forming fluids of the Longhua Ni-Co deposits were derived from circulating meteoric water and therefore should have had no genetic link to metamorphism. The Dishui granite (age 441.0 ± 3.6 Ma; unpublished data) near the Longhua ore field is younger than the Ni–Co arsenide–quartz–calcite veins, suggesting that the granite did not supply the heat for the circulating meteoric waters during the formation of the Ni-Co veins. The heat source was possibly the numerous Ordovician granites in the region (with age of 410–467 Ma, Wang et al., 2013 and reference therein).

The Re-Os isotope age of the Longhua high-grade Ni-Co vein ore is similar to those of MVT Pb-Zn deposits in the South China Block (Fig. 1; Cao et al., 2015; 2018; Du et al., 2018; Duan et al., 2014; Tan et al., 2018; Wang et al., 2018; Xiong et al., 2018; Yang et al., 2015; Yu et al., 2017), suggesting tha collision between the North China and South China blocks triggered the formation of the Caledonian MVT Pb-Zn deposits (Xiong et al., 2018) and the Longhua low temperature hydrothermal Ni-Co vein deposit.

#### 6.3.2. Implications for Ni solubility and mobility in low-temperature hydrothermal fluids

Ni is usually considered as the least soluble first-row transition metal in most common geological fluids (Liu et al., 2012) and that it is not easily remobilized by hydrothermal fluids (Le Vaillant et al., 2016). With a growing number of Ni deposits being identified as having a hydrothermal origin, it is increasingly accepted that Ni can be mobilized during hydrothermal alteration (Gonzalez-Alvarez et al., 2013; Keays and Jowitt, 2013; Kamenetsky et al., 2016). For example, experimental works on the brines of Mississippi Valley ore deposits has revealed that Ni can dissolve as chloride complexes in brines at 350 °C and 500 bars (Bischoff et al., 1981). Organic ligands have also been suggested to enhance Ni mobility in low-temperature and low-pressure systems (Tepper et al., 2001; Gonzalez-Alvarez et al., 2010). In addition, reduced fluids rich in $CO_2$, $CH_4$ and S are ideal for Ni transportation (e.g., Borovikov et al., 2008; Ahmed et al., 2009). Bicarbonate and $CO_2$ in fluids can enhance heavy metal leaching, which otherwise

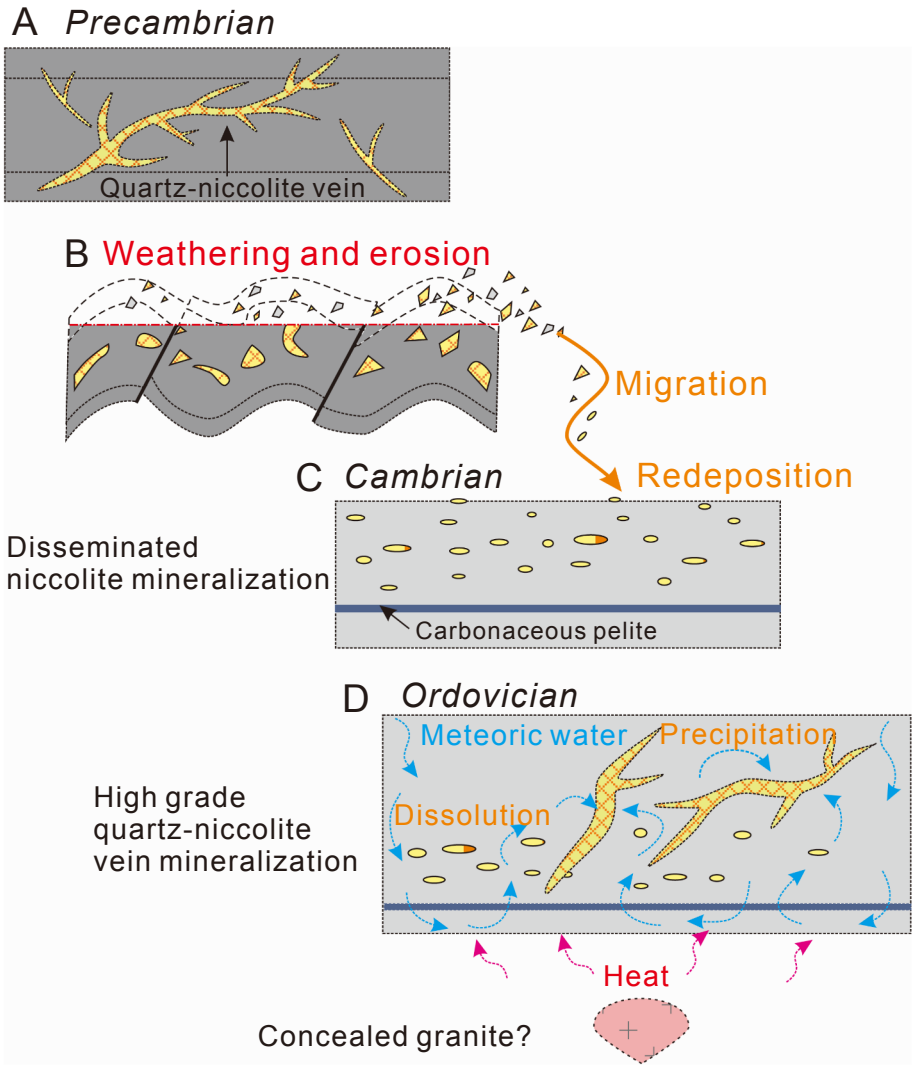


**Fig. 10.** Schematic showing the forming processes of the Longhua hydrothermal Ni-Co deposit.

would require higher temperatures (> 400 °C) for Ni extraction (e.g., Ellis, 1986; Reed, 1997; Pirajno, 2009). The hydrothermal Ni deposits considered in previous studies were generally formed at temperatures of 250–600 °C (Gonzalez-Alvarez et al., 2010). However, the solubility and mobility of Ni in fluids with temperatures of < 250 °C are poorly understood (Gonzalez-Alvarez et al., 2013). Nickel solubility in groundwater can yield concentrations of 195 ppm, predominantly in the form of free $Ni^{2+}$ (52%–63%) and $NiHCO_3^+$ (23%–32%) (Larsen and Postma, 1997), suggesting Ni can be transported in low temperature fluids (< 200 °C) under certain condition. Our study indicates that the Longhua Ni–Co vein ore bodies have high Ni concentrations and formed in a low-temperature (< 200 °C) and low-salinity (< 8.8 wt% NaCl equiv.) environment. This suggests that Ni can be dissolved and mobilized effectively in hydrothermal fluids with temperature lower than 200 °C. Since the fluids have low-salinity (< 8.8 wt% NaCl equiv.), chloride can be precluded as an important ligand in the solubility and mobility of Ni in the Longhua hydrothermal ore veins. Sulfides are rare in the Longhua Ni–Co deposit, similar to the Wittichen Ag–Bi–Co–Ni–U deposit (Staude et al., 2012), suggesting that S did not play an important role in the Longhua hydrothermal ore-forming fluids. Although organic matter can appropriate ligands to promote Ni mobility in low-temperature fluids (Greenwood et al., 2013), no organic matter has been found in the Longhua ore-forming fluids or associated with the ore veins, and therefore organic ligands should not be an important Ni-mobilizing agent in the Longhua Ni–Co deposit.

The Longhua Ni–Co arsenides–quartz–calcite veins are rich in arsenides and carbonate, suggesting that the ore-forming fluids were rich in $As^-$ and $HCO_3^-$ or $CO_3^{2-}$. Similarly, arsenides and carbonate minerals are common in Ni vein mineralization in many hydrothermal Ni deposit; e.g., the Miitel komatiite-hosted Ni-sulfide deposit, Yilgarn Craton, Western Australia (Le Vaillant et al., 2015), five-element deposits (Kissin, 1992), and the Bou Azzer ore (EnNaciri et al., 1997). The wide occurrence of this mineral assemblage, in combination with brine sediments in Mississippi containing 90 ppm Ni and 160 ppm As (Saunders and Rowan, 1990), indicates that Ni could be transported in low-temperature As-rich fluids.

We propose that Ni can be transported mainly as free $Ni^{2+}$ and $NiHCO_3^+$ in low-temperature (< 200 °C) arsenide and $HCO_3^-$ or $CO_3^{2-}$ rich reduced fluids.

### 6.3.3. Ore–forming processes

Bischoff et al. (1981) reported that the interaction between low-temperature fluids and carbonate-bearing rocks can produce $CO_2$ or $HCO_3^-$ rich fluids. Carbonaceous pelites are interbedded with the middle Cambrian Shuikoushan Group, which hosts the Longhua Ni-Co ores. Combining the geological and ore-forming fluid features, we suggest that the Longhua Ni–Co vein mineralization occurred as follows. (1) Precambrian quartz–niccolite mineralization (Fig. 10A) was dissolved and transported to the Longhua mineralization site (Fig. 10B), which formed disseminated niccolite mineralization in the Cambrian

source rocks (Fig. 10C). (2) Ordovician granitic magmatism in the region led to the meteoric fluids interacting with the carbonaceous pelites, which formed reduced, $HCO_3^-$ or $CO_3^{2-}$ rich fluids. The fluids dissolved the disseminated niccolite (Fig. 10D), and extracted As and Ni. (3) Niccolite and other Ni- and Co-bearing minerals were rapidly precipitated from the ore-forming fluids, in response to an abrupt change in the geochemical environment (e.g. oxygen fugacity), forming the high-grade Ni–Co vein mineralization (Fig. 10D). However, the main factors that resulted in the rapid precipitation of the Ni–Co arsenides are yet to be identified.

### 6.4. A new type of sedimentary hosted low temperature Ni deposit?

Since the discovery of the Avebury deposit in Tasmania, Australia, hydrothermal Ni deposits have attracted increasing attention (Gonzalez-Alvarez et al., 2013; Lisitsin et al., 2013). Most hydrothermal Ni deposits have genetic links to magmatic Ni-sulfide or ultramafic–mafic rocks (e.g., Gonzalez-Alvarez et al., 2013; Hofmann et al., 2014; Kamenetsky et al., 2016; Keays and Jowitt, 2013; Table 1). These Ni deposits are often spatially associated with magmatic Ni deposits or altered ultramafic–mafic rocks, and mostly contain Ni-sulfides as the main ore minerals (Table 1). Significantly, the Longhua Ni–Co deposit differs from these types of Ni deposit.

Another important type of hydrothermal Ni deposit is those hosted in sedimentary rocks that have no spatial relationship with magmatic Ni deposits or ultramafic–mafic rocks. These include: (1) black-shale-hosted deposits (Coveney and Nansheng, 1991; Lehmann et al., 2007; Mao et al., 2002; Xu et al., 2013; Orberger et al., 2003); (2) unconformity U-related deposits (Capistrant et al., 2015; Jefferson et al., 2007); and (3) five-element (Ag–U–Co–Ni–Bi) deposits (Kissin, 1992; Staude et al., 2012).

Black-shale-hosted deposits include those in South China (Jiang et al., 2006) and in Yukon, Canada (Orberger et al., 2003). These Ni deposits are hosted in organic-rich black shales (Horan et al., 1994; Coveney and Nansheng, 1991; Lehmann et al., 2007; Mao et al., 2002; Xu et al., 2013; Orberger et al., 2003). The deposits in South China are > 400 km from the Longhua deposit (Fig. 1) and are hosted in thin discontinuous phosphate-rich stratigraphic horizons (< 10 cm) of black shale that extends intermittent for > 1600 km along strike (Jiang et al., 2006). The ore bodies contain not only high Ni concentrations, but also high concentrations of PGE, Mo, Au, and Zn. The main Ni minerals are sulfides, including vaesite and bravoite, with minor millerite, polydymite, gersdorffite, pentlandite, and violarite (Jiang et al., 2006). The metal sources of these deposits are suggested to have been derived from the scavenging of seawater by organic material (Lehmann et al., 2007; Mao et al., 2002; Xu et al., 2013), or from submarine hydrothermal fluids (Coveney and Nansheng, 1991; Jiang et al., 2006; 2007; Jowitt and Keays, 2011; Pi et al., 2013). Nickel deposits in the Yukon are similar to the black-shale-hosted Ni deposits in South China, except that they are hosted in Upper Devonian black shales and are poor in Au and Mo (Orberger et al., 2003). In addition, some Co–Ni–Ba–As–Ag veins cut the Kupferschiefer black shale (Vaughan et al., 1989), which hosts Cu–Pb–Zn deposits in Germany and Poland. Nickel in these deposits occurs in arsenides, including rammelsbergite, bravoite, pentlandite, and millerite (Capistrant et al., 2015; Puttmann et al., 1988; Vaughan et al., 1989; Table 1). The Longhua Ni–Co deposit differs from these deposits in both ore mineral composition and element association.

A large amount of Ni mineralization is associated with unconformity U deposits such as those in the Athabasca Basin of Canada (Dahlkamp, 1978; Jefferson et al., 2007; Chi et al., 2019; Table 1). Nickel in these deposits resides manly in arsenides, such as gersdorffite, millerite, niccolite, and rammelsbergite, with some bravoite (Dahlkamp, 1978) and Ni–Bi minerals. These deposits were formed by paleo-weathering (Dahlkamp, 1978) or hydrothermal fluids rather than by magmatic fluids (Capistrant et al., 2015), and are similar to the Longhua deposit in their mineral assemblage; however, they have different element associations and geological settings.

Five-element (Ag–U–Co–Ni–Bi) deposits are characterized by veins hosted in igneous or sedimentary terranes with little or no volcanism (Kissin, 1992; Staude et al., 2012; Markl et al., 2016). The Ni mineralization is usually of extraordinary enrichment, and typically contains native Ag and Bi. The gangue minerals are usually dolomite and calcite (Kissin, 1992). Nickel and Co minerals are predominantly arsenides, including rammelsbergite, safflorite, niccolite, cloanthite, and maucherite (Kissin, 1992). Five-element deposits are similar to the Longhua Ni–Co deposit in their high Ni concentration and mineral assemblage; however, they usually contain native Ag and Bi, and their ore-forming fluids are of high saline (around 25 wt% NaCl + $CaCl_2$) (Staude et al., 2012; Markl et al., 2016), which differs from the Longhua Ni–Co deposit.

In addition to the hydrothermal Ni deposits discussed above, Ni potential in the central African sediment-hosted Cu–Co belt is attracting increasing attention (Steven and Armstrong, 2003). Nickel deposits in the ore belt occur mainly as stratiform Co–Ni–Cu mineralization (e.g., the Kalumbila prospect on the southeastern side of the Kabompo Dome, Zambia; Steven and Armstrong, 2003), U–Ni ore hosted within highly brecciated carbonate and siliciclastic sediments (e.g., the Shinkolobwe and Swambo deposits in the southern Democratic Republic of Congo; Capistrant et al., 2015), and Ni ores hosted within a sequence of quartz-, carbonate-, and carbon-rich metasedimentary rocks (e.g., the Enterprise deposit in Zambia; Capistrant et al., 2015). Nickel in these deposits resides primary in sulfides (e.g., pentlandite, violarite, siegenite, and millerite). The Ni source of these deposits is unclear, although rift-related hydrothermal or metamorphic fluids have been suggested (Steven and Armstrong, 2003).

In summary, The Longhua Ni–Co deposit differs greatly from the above hydrothermal Ni deposits in terms of (1) the paragenetic sequence of mineralization, that the Cambrain co-sedimentary disseminated low grade niccolite ore re-dissolved by post-sedimentary fluids forming the Ordovician high grade vein-type niccolite ore; (2) element assemblage and ore mineral composition, that mainly of Ni-Co arsenides; and (3) ore-forming fluids, which were $As^-$ and $HCO_3^+$/$CO_3^{2+}$ rich with temperature < 200 °C and salinity < 10 wt% (Table. 4). Although the key factors resulting in the precipitation of the high-concentration Ni ore are poorly known, the Longhua Ni–Co deposit appears to represent a new type of hydrothermal Ni ore hosted in sedimentary rocks, which is consistent with the prediction that there remains potential for new classes of hydrothermal Ni deposits to be discovered (Gonzalez-Alvarez et al., 2013).

## 7. Conclusions

Based on the above results and discussion, we present the following conclusions.

(1) The Longhua Ni–Co deposit was formed by early stage re-deposition of metals in sediments during the Cambrian that formed low-grade ore or source beds, and second-stage vein mineralization that formed high-grade Ni–Co ore bodies during the Ordovician (462.6 ± 8.5 Ma).
(2) The second-stage vein mineralization was formed from low-temperature (150–180 °C) low-salinity (1.2–8.8 wt% NaCl equiv.) fluids derived from circulating meteoric water.
(3) Arsenic- and $HCO_3^-$-rich low-salinity fluids, which formed from interactions among meteoric water, carbonaceous pelite, and Cambrian low-grade ore, promoted the solubility and mobility of Ni in a low-temperature environment.
(4) The Longhua Ni–Co vein mineralization differs greatly from other hydrothermal Ni mineralization in terms of mineralogy, ore mineral composition, element association, and ore-forming process, and may represent a new type of hydrothermal Ni–Co deposit hosted in sedimentary rocks.

**Table 4**
Summerized characterices of Longhua Ni-Co deposit and other types of hydrothermal Ni deposits hosted in sedimentary packages.

| Deposits | | Mineralization | Characteristic elements | Host rock | Ore minerals | Ore Fluids | | | | Reference |
|---|---|---|---|---|---|---|---|---|---|---|
| | | | | | | Source | Temperature (°C) | Salinity | | |
| Longhua Ni-Co deposit | South China | Dissmissed | Ni | Pelite with carbonaceous pelite interlayer | Niccolite | Unknown | Unknown | Unknown | | This study |
| | | Veins | Ni-Co | Siltstone with carbonaceous pelite interlayer | Arsenides | Meteoric water | 118–198 (peak at 150–182) | 1.2–8.8 wt% NaCl | | |
| Black shale hosted deposits | South China; Yukon | Thin discontinuous stratigraphic horizon | Ni, PGE, Mo, Au, and Zn | Black shales | Sulfides | Seawater/submarine hydrothermal fluids | Unknown | Unknown | | Orberger et al., 2003;Jiang et al., 2006; 2007; Lehmann et al., 2007 |
| | Spremberg-Weisswasser; Lower Silesia | Veins | Co, Ni, Ba, As and Ag | Kupferschiefer black shale | Sulfides and arsenides | | Unknown | Unknown | | Capistrant et al., 2015; Puttmann et al., 1988; Vaughan et al., 1989; |
| Unconformity-associated U deposits | Athabasca Basin | Lenses | U, Ni, Co, Cu, Pb, Zn, and Mo | Sandstone and conglomerate | Sulfide and arsenide | Basin brine | 180–250 | 20–30 wt% NaCl + $CaCl_2$ | | Dahlkamp, 1978; Jefferson et al., 2007; Chi et al., 2019 |
| Five element deposits | Wittichen, Schwarzwald; Wenzel, Schwarzwald | Veins | Ag, U, Co, Ni, Bi, Zn and Pb | Leucogranite, redbed | Arsenides | Basin brine | 150–250 | 20–28 wt% NaCl + $CaCl_2$ | | Kissin, 1992; Staude et al., 2012; Markl et al., 2016 |
| Central African Copperbelt | Kalumbila, Enterprise | Stratiform | Co-Ni-Cu | Carbonaceous metasedimentary | Sulfide | Metamorphic/rift-related hydrothermal fluids | 300–600 | Unknown | | Steven and Armstrong, 2003; Capistrant et al., 2015 |

## Declaration of Competing Interest

The authors declare that they have no known competing financial interests or personal relationships that could have appeared to influence the work reported in this paper.

## Acknowledgements

We are grateful to the Longhua ore company for fieldwork assistance. This work was supported by the National Natural Science Foundation of China (41772065, 41372084, 41502073). We thank Editor Peter C. Lightfoot and two anonymous reviewers for their helpful and constructive comments and advices to improve the earlier version of the manuscript. This is contribution No. IS-2812 from GIGCAS.

## Appendix A. Supplementary data

Supplementary data to this article can be found online at https://doi.org/10.1016/j.oregeorev.2020.103393.

## References

Ahmed, A.H., Arai, S., Ikenne, M., 2009. Mineralogy and Paragenesis of the Co-Ni Arsenide Ores of Bou Azzer, Anti-Atlas, Morocco. Econ. Geol. 104 (2), 249–266.

Arndt, N. T., Lesher, C. M., and Czamanske, G. K (2005) Mantle-derived magmas and magmatic Ni-Cu-(PGE) deposits. Economic Geology 100th Anniversary Volume: 5–24.

Baertschi, P., 1976. Absolute O-18 Content of Standard Mean Ocean Water. Earth Planet. Sci. Lett. 31 (3), 341–344.

Barnes, S. J., and Lightfoot, P. C (2005) Formation of magmatic nickel-sulfide ore deposits and processes affecting their copper and platinum-group element contents. Economic Geology 100th Anniversary Volume: 179–214.

Bischoff, J., Radtke, A.R., Rosenbauer, R., 1981. Hydrothermal alteration of greywacke by brine and seawater: role of alteration and chloride complexing on metal solubilization at 200 ° and 350 °C. Econ. Geol. 88, 123–138.

Bodnar, R.J., 1993. Revised Equation and Table for Determining the Freezing-Point Depression of H2o-Nacl Solutions. Geochim. Cosmochim. Acta 57 (3), 683–684.

Borovikov, A.A., Lebedev, V.I., Borisenko, A.S., 2008. Fluid regime of the formation of hydrothermal Ni-Co-As deposits and the involvement of ammonia in ore-forming process. Russian Mineralogy Society: Proceedings of XIII International Conference on Thermobarogeochemistry and IVth APIFIS Symposium. 2, 16–18.

Cao, L., Duan, Q.F., Zhou, Y., 2015. Rb-Sr dating of sphalerites from the Aozigang zinc deposit in Hubei Province and its geological significance. Geol. China 42 (1), 235–247.

Cao, L., Liang, Y.M., Duan, Q.F., Liu, C.P., Zhou, Y., 2018. Geological characteristics and Rb-Sr dating of sphalerites from the Shengtianping zincdeposit in Southeastern Yangtze Block and its geological significance. Geol. J. China Universities 24 (4), 504–515.

Capistrant, P.L., Hitzman, M.W., Wood, D., Kelly, N.M., Williams, G., Zimba, M., Kuiper, Y., Jack, D., Stein, H., 2015. Geology of the Enterprise Hydrothermal Nickel Deposit, North-Western Province, Zambia. Econ. Geol. 110 (1), 9–38.

Charvet, J., Lapierre, H., Yu, Y.W., 1994. Geodynamics significance of the Mesozoic volcanism of southeastern China. J. Southeast Asian Sci 9 (4), 387–396.

Charvet, J., Shu, L.S., Shi, Y.S., Guo, L.Z., Faure, M., 1996. The building of south China: collision of Yangtze and Cathaysia blocks, problems and tentative answers. J. SE Asian Earth Sci 13 (3–5), 223–235.

Charvet, J., Shu, L.S., Faure, M., Choulet, F., Wang, B., Lu, H.F., Breton, N.L., 2010. Structural development of the Lower Paleozoic belt of South China: Genesis of an intracontinental orogen. J. Asian Earth Sci 39 (4), 309–330.

Chen, N.S., Yang, X., Liu, D.H., Xiao, X.J., Fan, D.L., Wang, L.F., 1982. Lower Camgrian balck argillaceous and arenaceous rock serious in south Chan and its associated tratiform deposits. Mineral Deposits 2, 39–51.

Chen, X.L., Liang, H.Y., Richards, J.P., Huang, W.T., Zhang, J., Wu, J., Sotitiou, P., 2018. Age and granite association of skarn W mineralization at Niutangjie district, South China Block. Ore Geol. Rev. 102, 268–283.

Chen, A., 1999. Mirror thrusting in the south China Orogenic belt: tectonic evidence from western Fujian, southeastern China. Tectonophysics 305, 497–519.

Chi, G.X., Chu, H.X., Petts, D., Potter, E., Jackson, S., Williams-Jones, A., 2019. Uranium-rich diagenetic fluids provide the key to unconformity-related uranium mineralization in the Athabasca Basin. Sci. Rep. 9, 5530.

Clayton, R.N., Mayeda, T.K., 1963. The Use of Bromine Pentafluoride in the Extraction of Oxygen from Oxides and Silicates for Isotopic Analysis. Geochim. Cosmochim. Acta 27, 43–52.

Coleman, M.L., Shepherd, T.J., Durham, J.J., Rouse, J.E., Moore, G.R., 1982. Reduction of Water with Zinc for Hydrogen Isotope Analysis. Anal. Chem. 54 (6), 993–995.

Coveney Jr, R.M., Nansheng, C., 1991. Ni-Mo-PGE-Au-rich ores in Chinese black shales and speculations on possible analogues in the United States. Miner. Deposita 26, 83–88.

Dahlkamp, F.J., 1978. Geologic Appraisal of the Key Lake U-Ni Deposits, Northern

Saskatchewan. Econ. Geol. 73 (8), 1430–1449.
Du, G.M., Cai, H., Mei, Y.P., 2018. Application of Rb-Sr Isochron dating method in sphalerite of sulphide deposit–a case study from Dagoudong Pb-Zn deposit in Xinhuang, Western Hunan Province. Geol. Mineral Resour. South China 28 (2), 175–180.
Duan, Q.F., Cao, L., Zeng, J.L., Zhou, Y., Tang, Z.Y., Li, K., 2014. Rb-Sr dating of sphalerites from Shizishan Pb-Zn deposit in Huayuan ore concentration area, western Hunan, and its geological significance. Earth Sci. – J. China Univ. Geosci. 39 (8), 977–999.
EnNaciri, A., Barbanson, L., Touray, J.C., 1997. Brine inclusions for the Co-As(Au) Bou Azzer district, Anti-Atlas Mountains, Morocco. Econ. Geol. Bull. Soc. Econ. Geol. 92 (3), 360–367.
Elias, M., 2002. Nickel laterite deposits—geological overview, resources and exploitation. vol. 4. University of Tasmania, CODES Special Publication, pp. 205–220.
Ellis, A.J., 1986. Natural hydrothermal systems and experimental hot water/rock interaction: reactions with NaCl solutions and trace metal extraction. Geochim. Cosmochim. Acta 32, 1356–1363.
Gao, S., Ling, W.L., Qiu, Y., Zhou, L., Hartmann, G., Simon, K., 1999. Contrasting geochemical and Sm-Nd isotopic compositions of Archean metasediments from the Kongling high-grade terrain of the Yangtze craton: Evidence for cratonic evolution and redistribution of REE during crustal anatexis. Geochim. Cosmochim. Acta 63, 2071–2088.
Gao, P., Zheng, Y.F., Zhao, Z.F., 2017. Triassic granites in South China: a geochemical perspective on their characteristics, petrogenesis, and tectonic significance. Earth Sci. Rev 173, 266–294.
Gonzalez-Alvarez, I., Porwal, A., Beresford, S.W., McCuaig, T.C., Maier, W.D., 2010. Hydrothermal Ni prospectivity analysis of Tasmania, Australia. Ore Geol. Rev. 38 (3), 168–183.
Gonzalez-Alvarez, I., Pirajno, F., Kerrich, R., 2013. Hydrothermal nickel deposits: Secular variation and diversity. Ore Geol. Rev. 52, 1–3.
Greenwood, P.F., Brocks, J.J., Grice, K., Schwark, L., Jaraula, C.M.B., Dick, J.M., Evans, K.A., 2013. Organic geochemistry and mineralogy. I. Characterisation of organic matter associated with metal deposits. Ore Geol. Rev. 50, 1–27.
GXBGMR (Bureau of Geology and Mineral Resources of Guangxi Zhuang Autonomous Region) (1985) Regional Geology of the Guangxi Zhuang Autonomous Region. Geol. Publ. House, Beijing, pp. 1–853 (in Chinese with English abstract).
Horan, M.F., Morgan, J.W., Grauch, R.I., Coveney, R.M., Murowchick, J.B., Hulbert, L.J., 1994. Rhenium and Osmium Isotopes in Black Shales and Ni-Mo-Pge-Rich Sulfide Layers, Yukon-Territory, Canada, and Hunan and Guizhou Provinces, China. Geochimica Et Cosmochimica Acta 58 (1), 257–265.
Hsü, K.J., Li, J.L., Chen, H.H., Wang, Q.C., Sun, S., Sengör, A.M.X., 1990. Tectonics of south China: Key to tectonics of south China: Key to understanding west Pacific geology. Tectonophysics 193, 9–39.
Huang, J., Ren, J., Jiang, C., Zhang, Z., and Qin, D (1980) The Geotectonic Evolution of China, Science, Beijing, pp. 1–124.
Huang, W.T., Wu, J., Zhang, J., Liang, H.Y., Qiu, X.L., 2017. Geochemistry and Hf–Nd isotope characteristics and forming processes of the Yuntoujie granites associated with W–Mo deposit, Guangxi, South China. Ore Geol. Rev. 81 953–946.
Huang, W., Liang, H., Wu, L., Wu, J., Li, J., Bao, Z., 2018. Asynchronous formation of the adjacent epithermal Au-Cu and porphyry Cu-Mo deposits in the Zijinshan orefield, southeast China. Ore Geol. Rev. 102, 351–367.
Jefferson, C.W., Thomas, D.J., Gandhi, S.S., Ramaekers, P., Delaney, G., Brisbin, D., Cutts, C., Quirt, D., Portella, P., Olson, R.A., 2007. Unconformity-associated uranium deposits of the Athabasca Basin, Saskatchewan and Alberta. Geological Association of Canada, Mineral Deposits Division, Special Publication 5, 273–305.
Jiang, S.Y., Chen, Y.Q., Ling, H.F., Yang, J.H., Feng, H.Z., Ni, P., 2006. Trace- and rare-earth element geochemistry and Pb-Pb dating of black shales and intercalated Ni-Mo-PGE-Au sulfide ores in Lower Cambrian strata, Yangtze Platform, South China. Miner. Deposita 41 (5), 453–467.
Jiang, S. Y., Yang, J. H., Ling, H, F., Chen, Y. O., Feng, H, Z., Zhao, K, D., and Ni, P (2007) Extreme enrichment of polymetallic Ni-Mo-PGE-Au in Lower Cambrian black shales of South China: an Os isotope and PGE geochemical investigation. Palaeogeography, Palaeoclimatology, Palaeoecology 254, 217–228.
Pi, D.H., Liu, C.Q., Shields-Zhou, G.A., Jiang, S.Y., 2013. Trace and rare earth element geochemistry of black shale and kerogen in the early Cambrian Niutitang Formation in Guizhou province, South China: constraints for redox environments and origin of metal enrichments. Precambr. Res. 225, 218–229.
Jowitt, S.M., Keays, R.R., 2011. Shale-hosted Ni-(Cu-PGE) mineralization: a global overview. Appl. Earth Sci. 120, 187–197.
Kamenetsky, V.S., Lygin, A.V., Foster, J.G., Meffre, S., Maas, R., Kamenetsky, M.B., Goemann, K., Beresford, S.W., 2016. A story of olivine from the McIvor Hill complex (Tasmania, Australia): Clues to the origin of the Avebury metasomatic Ni sulfide deposit. Am. Mineral. 101 (5–6), 1321–1331.
Keays, R.R., Jowitt, S.M., 2013. The Avebury Ni deposit, Tasmania: A case study of an unconventional nickel deposit. Ore Geol. Rev. 52, 4–17.
Kissin, S.A., 1992. Five-element (Ni-Co-As-Ag-Bi) veins. Geosci. Canada 19 (3), 113–124.
Larsen, F., Postma, D., 1997. Nickel mobilization in a groundwater well field: Release by pyrite oxidation and desorption from manganese oxides. Environ. Sci. Technol. 31 (9), 2589–2595.
Le Vaillant, M., Barnes, S.J., Fiorentini, M.L., Miller, J., McCuaig, T.C., Muccilli, P., 2015. A Hydrothermal Ni-As-PGE Geochemical Halo Around the Miitel komatiite-Hosted Nickel Sulfide Deposit, Yilgarn Craton, Western Australia. Econ. Geol. 110 (2), 505–530.
Le Vaillant, M., Barnes, S.J., Fiorentini, M.L., Santaguida, F., Tormanen, T., 2016. Effects of hydrous alteration on the distribution of base metals and platinum group elements within the Kevitsa magmatic nickel sulphide deposit. Ore Geol. Rev. 72, 128–148.
Lehmann, B., Nagler, T.F., Holland, H.D., Wille, M., Mao, J.W., Pan, J.Y., Ma, D.S., Dulski, P., 2007. Highly metalliferous carbonaceous shale and Early Cambrian seawater. Geology 35 (5), 403–406.
Li, J.H., Dong, S.W., Cawood, P.A., Zhao, G.C., Johnston, S.T., Zhang, Y.Q., Xin, Y.J., 2018. An Andean-type retro-arc foreland system beneath northwest South China revealed by SINOPROBE profiling. Earth Planet. Sci. Lett 490, 170–179.
Li, X., McCulloch, M.T., 1996. Secular variation in the Nd isotopic composition of Neoproterozoic sediments from the southern margin of the Yangtze Block: Evidence for a Proterozoic continental collision in southeast China. Precambrian Res 76, 67–76.
Li, X.H., 2000. Cretaceous magmatism and lithosphere extension in southeast China. J. Asian Earth Sci 18, 293–305.
Li, Z.X., Li, X.H., 2007. Formation of the 1300-km-wide intracontinental orogen and postorogenic magmatic province in Mesozoic South China: a flat-slab subduction mode. Geology 35 (2), 179–182.
Li, Z.X., Li, X.H., Wartho, J.A., Clark, C., Li, W.X., Zhang, C.L., Bao, C.M., 2010a. Magmatic and metamorphic events during the Early Paleozoic Wuyi – Yunkai orogeny, southeastern south China: new age constraints and P – T conditions. Geol. Soc. Am. Bull 122 (5–6), 772–793.
Li, Z.H., X., J., Huang, Y., Zhang, S.L., 2010b. Types and genesis of nickel deposits in Guangxi. Territorial Resources in South China 2: 31–32 + 35.
Lightfoot, P.C., Stewart, R., Gribbin, G., Mooney, S.J., 2017. Relative contribution of magmatic and post-magmatic processes in the genesis of the Thompson Mine Ni-Co sulfide ores, Manitoba, Canada. Ore Geol. Rev. 83, 258–286.
Lisitsin, V.A., Gonzalez-Alvarez, I., Porwal, A., 2013. Regional prospectivity analysis for hydrothermal-remobilised nickel mineral systems in western Victoria, Australia. Ore Geol. Rev. 52, 100–112.
Liu, W.H., Migdisov, A., Williams-Jones, A., 2012. The stability of aqueous nickel(II) chloride complexes in hydrothermal solutions: Results of UV-Visible spectroscopic experiments. Geochim. Cosmochim. Acta 94, 276–290.
Liu, B. J., and X. S. Xu (1994) Atlas of Lithofacies and Palaeogeography of South China (Sinian to Triassic), Science, Beijing, 188 pp.
Loukola-Ruskeeniemi, K., Lahtinen, H., 2013. Multiphase evolution in the black-shale-hosted Ni-Cu-Zn-Co deposit at Talvivaara, Finland. Ore Geol. Rev. 52, 85–99.
Markl, G., Burisch, M., Neumann, U., 2016. Natural fracking and the genesis of five-element veins. Miner. Deposita 51 (6), 703–712.
Mao, J.W., Lehmann, B., Du, A., Zhang, G., Ma, D., Wang, Y., Zeng, M., Kerrich, R., 2002. Re-Os dating of polymetallic Ni-Mo-PGE-Au mineralization in Lower Cambrian black shales of South China and its geologic significance. Econ. Geol. 97, 1051–1061.
Ludwig, K.R., 2003. In: Isoplot/Ex, Version 3.0: A Geochronological Toolkit for Microsoft Excel. Geochronology Center, Special Publication, Berkeley.
Mao, J.W., Cheng, Y.B., Chen, M.H., Pirajno, F., 2013. Major types and time-space distribution of Mesozoic ore deposits in South China and their geodynamic settings. Miner. Deposita 48 (3), 267–294.
McKerrow, W.S., Scotese, C.R., Brasier, M.D., 1992. Early Cambrian continental reconstructions. Geol. Soc. [London] Journal 149, 599–606.
Melekestseva, I.Y., Zaykov, V.V., Nimis, P., Tret'yakov, G.A., Tessalina, S.G., 2013. Cu-(Ni-Co-Au)-bearing massive sulfide deposits associated with mafic-ultramafic rocks of the Main Urals Fault, South Urals: Geological structures, ore textural and mineralogical features, comparison with modern analogs. Ore Geol. Rev. 52, 18–36.
Orberger, B., Pasava, J., Gallien, J.P., Daudin, L., Pinti, D.L., 2003. Biogenic and abiogenic hydrothermal sulfides: controls of rare metal distribution in black shales (Yukon Territories, Canada). J. Geochem. Explor. 78–9, 559–563.
Peltonen, P., Kontinen, A., Huhma, H., Kuronen, U., 2008. Outokumpu revisited: New mineral deposit model for the mantle peridotite-associated Cu–Co–Zn–Ni–Ag–Au sulphide deposits. Ore Geol. Rev. 33 (3–4), 559–617.
Pirajno, F (2009) Hydrothermal Processes and Mineral Systems. Springer, Berlin, Germany. 1250 pp.
Pirajno, F., González-Álvarez, I., 2013. A re-appraisal of the Epoch nickel sulphide deposit, Filabusi Greenstone Belt, Zimbabwe: A hydrothermal nickel mineral system? Ore Geol. Rev. 52, 58–65.
Puttmann, W., Hagemann, H.W., Merz, C., Speczik, S., 1988. Influence of Organic Material on Mineralization Processes in the Permian Kupferschiefer Formation. Poland. Organic Geochemistry 13 (1–3), 357–363.
Qi, L., Zhou, M.-F., Gao, J., Zhao, Z., 2010. An improved Carius tube technique for determination of low concentrations of Re and Os in pyrites. J. Anal. Atom. Spectrom. 25, 585–589.
Qiu, Y.M., Gao, S., McNaughton, N.J., Groves, D.I., Ling, W., 2000. First evidence of > 3.2 Ga continental crust in the Yangtze craton of south China and its implications for Archean crustal evolution and Phanerozoic tectonics. Geology 28, 11–14.
Reed, M.H., 1997. Hydrothermal alteration and its relationship to ore fluid composition. In: Barnes, H.I. (Ed.), Geochemistry of Hydrothermal Ore Deposits, 3rd Edition. Wiley, pp. 303–365.
Roedder, E., 1984. In: Fluid Inclusions: Reviews in Mineralogy. vol. 12. Mineralogical Society of America, pp. 1–644.
Selby, D., Creaser, R.A., 2001. Re–Os geochronology and systematics in molybdenite from the Endako porphyry molybdenum deposit, British Columbia, Canada. Econ. Geol. Bull. Soc. Econ. Geol. 96 (1), 197–204.
Smoliar, M.I., Walker, R.J., Morgan, J.W., 1996. Re-Os ages of group IIA, IIIA, IVA, and IVB iron meteorites. Science 271 (5252), 1099–1102.
Staude, S., Werner, W., Mordhorst, T., Wemmer, K., Jacob, D.E., Markl, G., 2012. Multi-stage Ag–Bi–Co–Ni–U and Cu–Bi vein mineralization at Wittichen, Schwarzwald, SW Germany: geological setting, ore mineralogy, and fluid evolution. Miner. Deposita 47 (3), 251–276.
Stein, H.J., Morgan, J.W., Scherstén, A., 2000. Re-Os dating of low-level highly radiogenic (LLHR) sulfides: The Harnäs gold deposit, southwest Sweden, records

continental-scale tectonic events. Econ. Geol. 95, 1657–1671.
Steiner, M., Wallis, E., Erdtmann, B.D., Zhao, Y., Yang, R., 2001. Submarine-hydrothermal exhalative ore layers in black shales from South China and associated fossils—Insights into Lower Cambrian facies and bioevolution. Palaeogeogr. Palaeoclimatol. Palaeoecol. 169, 165–191.
Steven, N., Armstrong, R., 2003. A metamorphosed proterozoic carbonaceous shale-hosted Co–Ni–Cu deposit at Kalumbila, Kabompo dome: The Copperbelt ore shale in northwestern Zambia. Econ. Geol. Bull. Soc. Econ. Geol. 98 (5), 893–909.
Tan, J.J., Liu, C.P., Yang, H.M., Cai, Y.X., Lu, S.S., 2018. Geochronology and ore-forming material source constraints for Rouxianshan Pb-Zn deposit in Huayuan ore concentration area, western Hunan. Earth Scienc 43 (7), 2438–2448.
Tepper, J.H., Groddman, A.R., Crossey, L.J., Asmerom, Y., 2001. Influence of seasonal redox variations on mobility of trace metals in a shallow alluvial aquifer. Jemez Mountains, NM. American Geophysical Union, Fall Meeting, Abstract H51C–0340.
Vaughan, D.J., Sweeney, M., Friedrich, G., Diedel, R., Haranczyk, C., 1989. The Kupferschiefer – an Overview with an Appraisal of the Different Types of Mineralization. Econ. Geol. 84 (5), 1003–1027.
Wang, X.L., Zhou, J.C., Qiu, J.S., Zhang, W.L., Liu, X.M., Zhang, G.L., 2006. LA-ICP-MS U-Pb zircon geochronology of the Neoproterozoic igneous rocks from northern Guangxi, south China: Implications for tectonic evolution. Precambrian Res 145 (1–2), 111–130.
Wang, J., Li, Z.X., 2003. History of Neoproterozoic rift basins in South China: implications for Rodininia break-up. Precambrian Res 122 (1–4), 141–158.
Wang, S.W., Jin, C.H., Zhang, Y., Sun, X.M., Zhou, Q., Liao, Z.W., Guo, Y., Jiang, X.F., Wang, Z.Z., 2018. Sphalerites from the giant Wuzhishan Pb-Zn deposit in Guizhou: Rb-Sr dating and its geological implications. Sedimentary Geology and Tethyan Geology 38 (3), 78–87.
Wang, Y.J., Zhang, F.F., Fan, W.M., Zhang, G.W., Chen, S.Y., Gawood, P.A., Zhang, A.M., 2010. Tectonic setting of the Souch China Block in the early Paleoxoic: Resolving intracontinental and ocean closure models from detrital zircon U-Pb geochronology. Tectonics 29, TC6020.
Wang, Y.J., Fan, W.M., Zhang, G.W., Zhang, Y.H., 2013. Phanerozoic tectonics of the South China block: key observations and controversies. Gondwana Res 23, 1273–1305.
Wu, J., Liang, H.Y., Huang, W.T., Wang, C.L., Sun, W.D., Sun, Y.L., Li, J., Mo, J.H., Wang, X.Z., 2012. Indosinian isotope ages of plutons and deposits in southwestern Miaoershan-Yuechengling, northeastern Guangxi and implications on Indosinian mineralization in South China. Chin. Sci. Bull. 57, 1024–1035.
Xiong, S.F., Gong, Y.J., Jiang, S.Y., Zhang, X.J., Li, Q., Zeng, G.P., 2018. Ore genesis of the Wusihe carbonate-hosted Zn-Pb deposit in the Dadu River Valley district, Yangtze Block, SW China: evidence from ore geology, S-Pb isotopes, and sphalerite Rb-Sr dating. Miner. Deposita 53, 967–979.
Xu, L.G., Lehmann, B., Mao, J.W., 2013. Seawater contribution to polymetallic Ni-Mo-PGE-Au mineralization in Early Cambrian black shales of South China: Evidence from Mo isotope, PGE, trace element, and REE geochemistry. Ore Geol. Rev. 52, 66–84.
Xu, C., Rong, J.Y., Mitchell, C.E., Happer, D.A.T., Fan, J.X., Zhan, R.B., Zhang, Y.D., Li, R.Y., Wang, Y., 2000. Late Ordovician to earliest Silurian graptolite and brachiopod zonation from Yangtze region, south China with a global correlation. Geol. Mag 137 (6), 623–650.
Yang, H.M., Liu, C.P., Duan, R.C., Gu, X.M., Lu, S.S., Tan, J.J., Cai, Y.X., Zhang, L.G., Qiu, X.F., 2015. Rb-Sr and Sm-Nd isochron ages of Bokouchang Pb-Zn deposit in Tongren, Guizhou Province and their geological implication. Geotectonica et Metallogenia 10, 855–865.
Yu, Y.S., Liu, A.S., Dai, P.Y., Zhao, W.Q., Tao, M., Liu, Z.P., 2017. The metallogenic epoch and ore-forming material source of the Tang-bian Pb-Zn deposit in Tongren, Guizhou Province: Evidence from Rb-Sr dating of sphalerites and S-Pb isotope. Geological Bulletin of China 36 (5), 885–892.
Zheng, J.P., Griffin, W.L., Reilly, S.Y.O., Zhang, M., Pearson, N., 2006. Widespread Archean basement beneath the Yangtze craton. Geology 34, 417–420.
Zhu, M.Y., Zhang, J.M., Steiner, M., Yang, A.H., Li, G.X., Erdtmann, B.D., 2003. Sinian-Cambrian stratigraphic framework for shallow- to deep-water environments of the Yangtze Platform: an integrated approach. Prog. Nat. Sci 13, 951–960.